

See discussions, stats, and author profiles for this publication at: <https://www.researchgate.net/publication/49706058>

# SiC<sub>2</sub> Silagraphene and Its One-Dimensional Derivatives: Where Planar Tetracoordinate Silicon Happens

ARTICLE in JOURNAL OF THE AMERICAN CHEMICAL SOCIETY · FEBRUARY 2011

Impact Factor: 12.11 · DOI: 10.1021/ja107711m · Source: PubMed

---

CITATIONS

60

---

READS

59

## 4 AUTHORS, INCLUDING:



[Yafei Li](#)

Nanjing Normal University

48 PUBLICATIONS 2,052 CITATIONS

[SEE PROFILE](#)



[Zhen Zhou](#)

Nankai University

213 PUBLICATIONS 6,996 CITATIONS

[SEE PROFILE](#)



[Zhongfang Chen](#)

University of Puerto Rico at Rio Piedras

221 PUBLICATIONS 8,056 CITATIONS

[SEE PROFILE](#)

# $\text{SiC}_2$ Silagraphene and Its One-Dimensional Derivatives: Where Planar Tetracoordinate Silicon Happens

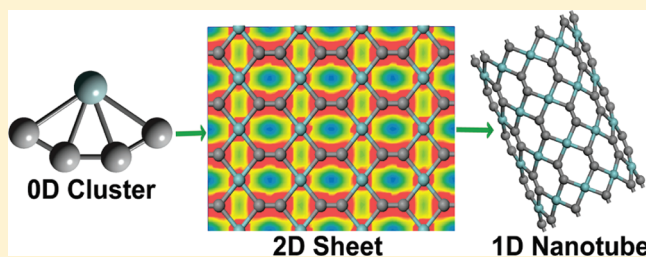
Yafei Li,<sup>†</sup> Fengyu Li,<sup>‡</sup> Zhen Zhou,<sup>\*,†</sup> and Zhongfang Chen<sup>\*,‡</sup>

<sup>†</sup>Institute of New Energy Material Chemistry, Key Laboratory of Advanced Energy Materials Chemistry (Ministry of Education), Tianjin Key Laboratory of Metal and Molecule Based Material Chemistry, Nankai University, Tianjin 300071, China

<sup>‡</sup>Department of Chemistry, Institute for Functional Nanomaterials, University of Puerto Rico, Rio Piedras Campus, San Juan 00931, Puerto Rico

Supporting Information

**ABSTRACT:** The periodic systems containing planar tetracoordinate silicon (ptSi),  $\text{SiC}_2$  silagraphene, nanotubes, and nanoribbons, were predicted by means of density functional theory (DFT) computations. In  $\text{SiC}_2$  silagraphene, each silicon atom is bonded by four carbon atoms in a pure plane, representing the first anti-van't Hoff/Lebel species in the Si-containing extended system.  $\text{SiC}_2$  nanotubes, rolled up by the  $\text{SiC}_2$  silagraphene, exhibit excellent elastic properties. All these ptSi-containing nanomaterials are metallic, regardless of the chirality, tube diameter, or ribbon width. The high stabilities of these systems strongly suggest the feasibility for their experimental realizations.



## 1. INTRODUCTION

As one of the most popular and important elements, carbon in known materials often has tetrahedral tetracoordination (as in diamond) or planar tricoordination (as in graphite) arrangements. In the past two decades, from graphite to fullerene<sup>1</sup> and carbon nanotubes,<sup>2,3</sup> carbon has displayed the versatility of  $\text{sp}^2$  hybridization coupled with the right valence. In particular, the newly realized single-layered graphite, graphene,<sup>4</sup> has dictated many intriguing structures and properties of carbon materials.<sup>5–11</sup>

Besides the normal  $\text{sp}^2$  and  $\text{sp}^3$  hybridization, in 1970, Hoffmann, Alder, and Wilcox<sup>12</sup> first argued the possible existence of “planar tetracoordinate carbon” (ptC) (known as the anti-van’t Hoff/Lebel<sup>13</sup> compound). Inspired by this fantastic idea, in 1976, Collins et al.<sup>14</sup> identified the first molecules with ptC by systematic computations. Experimentally, Cotton and Millar synthesized the first ptC compound in 1977,<sup>15</sup> although the unique bonding situation escaped the attention of the original authors.<sup>16</sup> Ever since, numerous ptC-containing molecules have been computationally designed, and many have been experimentally characterized;<sup>17</sup> even the existence of planar carbon with higher coordination has been actively pursued since the beginning of the 21st century.<sup>18,19</sup>

Silicon is in the same row of the periodic table as carbon, and both of them have four valence electrons. However, silicon has bonding characters strikingly different from those of carbon, especially for the possibility to form multiple bonds and hypercoordinate systems: while carbon has the genius to activate one p electron at a time, adopting, in turn,  $\text{sp}$ ,  $\text{sp}^2$ , and  $\text{sp}^3$  hybridization, respectively, to easily form multiple bonds, only few

examples of multiple bond silicon systems exist;<sup>20</sup> silicon can readily form five- and six-coordinate complexes,<sup>21</sup> while, in stark contrast, rare examples of hypercoordinate carbon molecules<sup>22</sup> are available. The intensive studies of ptC also captivated scientists to explore molecules with planar tetracoordinate silicon (ptSi) and its even higher coordinate analogues. Unfortunately, the early attempts to realize ptSi were not successful. Orthosilicic acid ester, the first molecule containing a ptSi center, was computationally predicted by Schleyer et al.<sup>23</sup> and experimentally reported by Meyer et al.<sup>24</sup> in 1979; however, the experimental reasoning was later questioned.<sup>25</sup> Tetraazafenestrane was predicted as another candidate for ptSi,<sup>26</sup> but the attempts to synthesize this type of compounds failed.<sup>27</sup>

Several groups computationally designed and searched for ptSi and planar hypercoordinate silicon compounds. Schleyer et al.<sup>28</sup> pointed out that a “one-sided”  $C_{2v}$  geometry for  $\text{SiLi}_4$  seems probable, and Belanzoni et al.<sup>29</sup> suggested the existence of a planar  $\text{Si}(\text{CO})_4$ . Tiznado et al.<sup>30</sup> recommended  $\text{Si}_5\text{Li}_7^+$ , a global minimum and a perfect seven-peak star-like structure featuring five ptSi subunits, as the synthesis target. Gribanova et al.<sup>31</sup> proposed to stabilize ptSi in borane clusters, while Islas et al. recommended to utilize boron rings to enclose planar hypercoordinate group 14 elements.<sup>32</sup> Szieberth et al.<sup>33</sup> advocated to use the  $\pi$  push–pull arrangement around the silicon to stabilize ptSi in orthosilicic ester and suggested to use ptSi as a new building block for conjugated

Received: August 26, 2010

Published: December 23, 2010

Si-containing systems. Li et al. designed ptSi at the center of the perfectly squared  $D_{4h}$   $M_4Cl_4Si$  ( $M = \text{Ni, Pd, or Pt}$ )<sup>34</sup> and a similar approach can also be used to stabilize planar hypercoordinate main group atoms centered in hexagonal hydrocopper complexes.<sup>35</sup> Li et al.<sup>36</sup> also proposed a unified structural pattern to incorporate planar tetra-, penta-, hexa-, hepta-, and octacoordinate silicon in  $C_{2v}$   $B_nE_2Si$  series ( $E = \text{CH, BH, or Si}$ ;  $n = 2-5$ ), and a series of S-shaped or cyclic  $(B_nE_mSi)_2H_2$  molecules. Noticeably, the joint computational and experimental efforts by Boldyrev et al.<sup>37</sup> led to the first and so far the only available observation of a ptSi molecule,  $\text{SiAl}_4^-$ , which has a planar structure and represents the simplest molecule to contain a ptSi. However, there are still relatively few studies on the “planar chemistry” of silicon as compared with planar hypercoordinate carbon chemistry, although planar tetra-coordination is fundamentally easier to realize with silicon than with carbon.<sup>38</sup>

Recently, extended systems with ptCs have been attracting much research interest. Pancharatna et al.<sup>39</sup> proposed a variety of extended networks with the stoichiometry of  $C_xM_x$  ( $M = \text{Be, Pt, or Zn}$ ,  $x = 1$ ;  $M = \text{Li}$ ,  $x = 2$ ) inspired by the existence of the  $C_5^{2-}$  local minimum with a ptC linking two three-membered rings.<sup>40</sup> These solids have relatively large band gaps, suggesting semiconducting or insulating behavior. Yang et al.<sup>41</sup> predicted the extended sandwich structures based on  $\text{CaAl}_4^{2-}$ . Especially, inspired by the intensive studies of carbon nanotubes and graphene, ptC-containing low-dimensional nanostructures have also been explored. Zhang et al.<sup>42</sup> constructed four kinds of zigzag boron–carbon nanotubes with ptC atoms, and the very small HOMO (highest occupied molecular orbital)–LUMO (lowest unoccupied molecular orbital) gaps of these finite-length tubes indicate the metallic character for their longer analogues. Wu et al.<sup>43,44</sup> designed families of ptC-containing flat, tubular, and cage supramolecular structures. Zeng and co-workers<sup>45</sup> demonstrated that the infinite ptC strip can be realized in Cu-decorated zigzag graphene nanoribbons. Motivated by a recently predicted ptC molecule,  $\text{CB}_4$ ,<sup>46</sup> Wu et al.<sup>47</sup> designed the two-dimensional (2D)  $B_2C$  graphene sheet and the one-dimensional (1D)  $B_2C$  nanotubes and nanoribbons, in which each carbon atom is bonded with four boron atoms, forming a ptC moiety.

The active quest for ptSi compounds and ptC-containing extended systems by peers, as well as our own finding of a  $\text{SiC}_4$  ( $C_{2v}$ ) local minimum (vide infra), prompted us to develop the planar tetracoordinate silicon into solids. To our best knowledge, no attempt in this regard has been reported. In particular, the unique properties of graphene and its 1D derivatives bring about an interesting question, what would happen when the ptSi is embedded into the 2D graphitic or 1D tubular and ribbon systems? Considering the many important applications of nanosilicon species, especially in semiconductor industry, these ptSi-containing nanostructures will not only enrich the basic science and advance the silicon-based technology, but also open up a new direction in nanosilicon research.

In this work, first, we confirmed that  $\text{SiC}_4$  molecule ( $C_{2v}$ ) is a local minimum structure containing a ptSi. On the basis of  $\text{SiC}_4$ , we designed a new type of 2D inorganic material, named  $\text{SiC}_2$  silagraphene. Like graphene, 2D  $\text{SiC}_2$  silagraphene could also be rolled into 1D  $\text{SiC}_2$  nanotubes or cut into 1D  $\text{SiC}_2$  nanoribbons. In  $\text{SiC}_2$  silagraphene and its 1D derivatives (nanotubes and nanoribbons), each Si atom is bonded with four carbon atoms to form a ptSi moiety. The structures, energetics, electronic and elastic properties, and a clear picture of the bonding characteristics for  $\text{SiC}_2$  silagraphene, nanotubes, and nanoribbons were revealed

by systematic density functional theory (DFT) computations, and a promising approach to achieve  $\text{SiC}_2$  sheet was also proposed.

## 2. COMPUTATIONAL DETAILS

For  $\text{SiC}_4$  molecule, full geometry optimizations, frequency analyses, as well as electronic structure computations were performed at the B3LYP<sup>48</sup> and the second-order Moller–Plesset (MP2)<sup>49</sup> levels of theory together with the 6-311+G\* basis set by using the Gaussian 03 package.<sup>50</sup>

For  $\text{SiC}_2$  silagraphene, nanotubes, and nanoribbons, our DFT computations employed an all-electron method within a generalized gradient approximation (GGA) for the exchange-correlation term, as implemented in the DMol<sup>3</sup> code.<sup>51</sup> The double numerical basis set including d polarization (DND) and PW91 functional<sup>52</sup> were adopted. Self-consistent field (SCF) calculations were conducted with a convergence criterion of  $10^{-6}$  au on the total energy and the electron density. To ensure high-quality computations, the real-space global orbital cutoff radius was chosen to be 5.1 Å. For 2D  $\text{SiC}_2$  silagraphene, we set the x and y directions parallel and the z direction perpendicular to the silagraphene plane, and we adopted a supercell length of 15 Å in the z direction. For  $\text{SiC}_2$  nanotubes and nanoribbons, 1D periodic boundary condition (PBC) was applied along the z direction to simulate their infinitely long systems. The minimum distance between two tubes (ribbons) is larger than 15 Å, which can safely avoid the interaction between two tubes (ribbons). The Brillouin zone was sampled with a  $6 \times 6 \times 1$  and  $1 \times 1 \times 10$   $\Gamma$  centered  $k$  points grid for 2D and 1D systems, respectively.

We evaluated the strain energies,  $E_s$ , for a variety of  $\text{SiC}_2$  nanotubes.  $E_s$  is defined as the difference in cohesive energy between tubular and graphitic structures, or the energy cost to wrap up a silagraphene sheet into a tube.

$$E_s = \frac{1}{n_{\text{NT}}} E_{\text{NT}}^{\text{tot}} - \frac{1}{3} E_{\text{sheet}}^{\text{tot}}$$

where  $n_{\text{NT}}$  is the number of atoms in the NT unit cell. The strain energies of other nanotubes were computed similarly. According to this definition, a lower stain energy means an easier process to form a tube from a planar sheet.

To evaluate the stability of different materials consisting of Si and C, the binding energy,  $E_b$ , was computed.  $E_b$  is defined as  $E_b = (xE_{\text{Si}} + yE_{\text{C}} - E_{\text{Si}_x\text{C}_y})/(x+y)$ , where  $E_{\text{Si}}$ ,  $E_{\text{C}}$ , and  $E_{\text{Si}_x\text{C}_y}$  are the energies of silicon, carbon atom, and the  $\text{Si}_x\text{C}_y$  nanomaterial, respectively. According to this definition, those with larger binding energies are more favorable energetically.

Molecular dynamics (MD) simulations were performed to assess the thermal stability of  $\text{SiC}_2$  silagraphene. PW91 functional and DND basis set were used, as implemented in the DMol<sup>3</sup> code. The initial configuration of  $\text{SiC}_2$  layer was annealed at different temperatures. At each temperature, MD simulation in NVT ensemble lasted for 10 ps with a time step of 1.0 fs. The temperature was controlled by using the Nosé–Hoover method.<sup>53</sup>

The elastic properties of  $\text{SiC}_2$  nanotubes were evaluated by computing their Young's modulus ( $Y_s$ ) as proposed by Hernández et al.,<sup>54</sup> which is defined as:

$$Y_s = \frac{1}{S_0} \left( \frac{\partial^2 E}{\partial^2 \varepsilon} \right)_{\varepsilon=0}$$

where  $S_0$  is the surface area of the nanotube at the zero strain, defined as  $S_0 = \pi D c_0$ ,  $E$  is the strain energy,  $c_0$  is the unit-cell length of the supercell, and  $\varepsilon$  is the axial strain.

## 3. RESULTS AND DISCUSSION

### 3.1. $\text{SiC}_4$ —An Inspiring ptSi Molecule for Extended Systems.

What motivated our search for extended ptSi-containing systems is the finding of the ptSi-containing  $\text{SiC}_4$  local minimum (Figure 1),

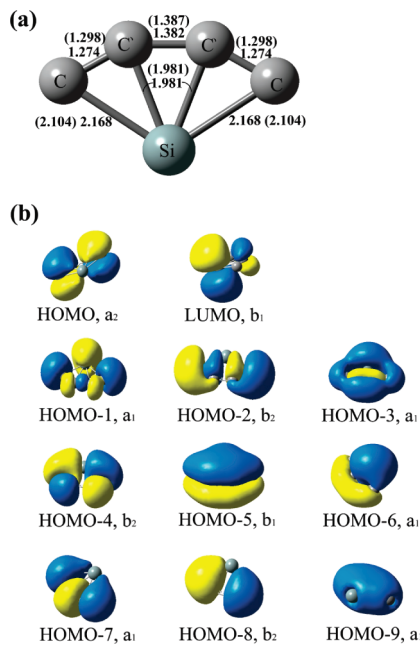


**Figure 1.** (a) B3LYP/6-311+G\* optimized structure of  $\text{SiC}_4$  molecule. The distances are in angstroms. The number in bracket is computed from MP2 procedure. (b) Canonical molecular orbitals (MOs) of  $\text{SiC}_4$ . The symmetries of the MOs are also given.

which has the lowest vibrational frequency of  $87.0 \text{ cm}^{-1}$  at the B3LYP/6-311+G\* level of theory. Like some previously reported ptSi molecules, such as  $\text{SiLi}_4$ ,<sup>28</sup> and  $\text{B}_n\text{E}_2\text{Si}$  series ( $\text{E} = \text{CH, BH, or Si; } n = 2-5$ ),<sup>36</sup>  $\text{SiC}_4$  also has  $C_{2v}$  symmetry. In  $\text{SiC}_4$ , the Si—C and Si—C' (as labeled in Figure 1a, C' represents the top two C atoms in the structure) bond lengths are 2.163 and 1.978 Å, respectively; the C—C' and C'—C' bond lengths are 1.274 and 1.382 Å, respectively. The second-order Moller-Plesset (MP2)<sup>55</sup> procedure gives nearly the same geometric structure as B3LYP.

To help understand the bonding characteristics of  $\text{SiC}_4$ , we calculated the natural population analysis (NPA) charges and the Wiberg bond index (WBI) based on natural bonding orbital (NBO) computations at the B3LYP/6-311+G\* level of theory. The Si atom is positively charged (NPA charge 1.25), while the C atoms are negatively charged (NPA charges for the peripheral C and C' atoms are -0.21 and -0.41, respectively). Correspondingly, the natural electron configurations for Si, C, and C' atoms are  $3s^{1.75} 3p_x^{0.14} 3p_y^{0.38} 3p_z^{0.46}$ ,  $2s^{1.52} 2p_x^{0.77} 2p_y^{1.11} 2p_z^{0.80}$ , and  $2s^{0.96} 2p_x^{1.15} 2p_y^{1.17} 2p_z^{1.08}$ , respectively. Clearly, the 3s orbital does not well hybridize with 3p for Si as compared with the 2s and 2p orbitals for C, due to the large energy separation between 3s and 3p orbitals. The computed WBIs for Si—C, Si—C', C—C', and C'—C' bonds are 0.42, 0.35, 2.27, and 1.21, respectively. These indicate that partial bonds form between ptSi atom and its surrounding C atoms, while the C—C' interactions have obviously double bond characteristics.

Scrutinizing the molecular orbitals can further help us understand how a ptSi is stabilized in  $\text{SiC}_4$  (Figure 1b). The HOMO is a delocalized  $\pi$  orbital, involving the p orbitals of peripheral C atoms. The HOMO-2  $\pi$  orbital is distributed on the two C—C' subunits of  $\text{SiC}_4$ . Both HOMO-5 and HOMO-6 are highly delocalized  $\sigma$  orbitals in the molecular plane, which also plays an important role in keeping the Si center and the peripheral carbon

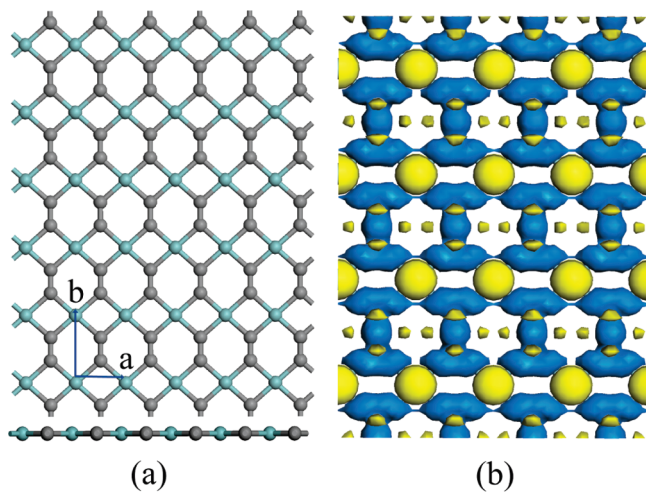


**Figure 2.** (a) Top (upper) and side (lower) views of geometric structure of 2D infinite  $\text{SiC}_2$  silagraphene. The lattice vectors  $a$  and  $b$  are denoted. (b) The deformation electronic density of  $\text{SiC}_2$  silagraphene. Blue and yellow refer to electron-rich and -deficient area, respectively. The isosurface value is 0.05 e/Å<sup>3</sup>.

atom in the same plane. Interestingly, the LUMO of  $\text{SiC}_4$  corresponds to the destabilizing lone pair electrons of Si in a ptSi arrangement. Similar to the case for the ptC compounds,<sup>56</sup> removing the destabilizing ptSi lone pair electrons significantly stabilizes the ptSi arrangement.

Note that this ptSi-containing  $\text{SiC}_4$  isomer is not the global minimum. We searched numerous isomers at the potential energy surface and found that the global minimum is a linear structure, which is about 1.268 eV at B3LYP/6-311+G\* (0.708 eV at MP2/6-311+G\*) lower in energy than the ptSi isomer (see the Supporting Information). However, this ptSi-containing  $\text{SiC}_4$  local minimum does inspire us to design  $\text{SiC}_2$  silagraphene and its one-dimensional derivatives.

**3.2. Structural and Electronic Properties of  $\text{SiC}_2$  Silagraphene.** Encouraged by the above ptSi moiety, we designed a new 2D planar structure,  $\text{SiC}_2$  silagraphene, on the basis of the  $\text{SiC}_4$  building block. The structure of  $\text{SiC}_2$  silagraphene, optimized without any symmetry constraint, is purely planar (Figure 2a). The optimized lattice parameters, labeled as “ $a$ ” and “ $b$ ” (Figure 2a), are  $a = 2.864 \text{ Å}$  and  $b = 3.879 \text{ Å}$ , respectively. As compared with graphene whose unit cell contains two carbon atoms, the unit cell of  $\text{SiC}_2$  silagraphene contains one Si atom and two carbon atoms. In  $\text{SiC}_2$  silagraphene, each Si atom binds four carbon atoms to form a ptSi moiety, while each carbon atom is bound with two ptSi atoms and one carbon atom. Consequently, two neighboring  $\text{SiC}_4$  motifs in  $\text{SiC}_2$  silagraphene share two same carbon atoms in the  $a$  direction and are linked with two C—C bonds in the  $b$  direction. In  $\text{SiC}_2$  silagraphene, the SiC length (1.916 Å) is only a little longer than the standard Si—C single bond (1.87–1.91 Å),<sup>57</sup> while the CC bond length (1.332 Å) is equal to that of the C=C bond in ethylene (computed at our GGA-PW91 level).

To elucidate the nature of chemical bonding, we plotted the deformation charge density of  $\text{SiC}_2$  silagraphene by subtracting the charge density of isolated Si and C atoms from the sheet (Figure 2b). Obviously, some electrons are extracted from the 3p orbital of the ptSi atom and delocalized over four Si—C bonds, as implied by the yellow regions. The significant electron transfer from the Si atoms in  $\text{SiC}_2$  silagraphene (the net Mulliken charge on Si and C is 1.28 and -0.64 |e|, respectively) is similar to the

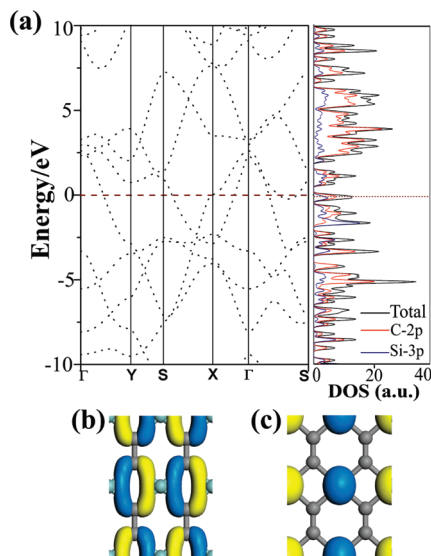


**Figure 3.** (a) Electronic band structure (left) and density of states (DOS, right) of  $\text{SiC}_2$  silagraphene. (b) The highest occupied electronic state and (c) the lowest unoccupied electronic state of  $\text{SiC}_2$  silagraphene at the  $\Gamma$  point. The isosurface value is 0.05 e/au.

case in the  $\text{SiC}_4$  molecule. Pronounced charge overlap is also observed between two neighboring carbon atoms, which are connected by a standard  $\text{C}=\text{C}$  bond. In  $\text{SiC}_2$  silagraphene, one  $\text{C}=\text{C}$  bond and its four neighboring Si atoms just resemble the structure of ethylene, which strongly prefers a planar molecule. Therefore, we can argue that it is the planarity-preferred ethylene-like skeletons that give rise to a planar  $\text{SiC}_2$  network, which is also supported by our analysis to the fenestrane-like cluster model (vide post).

Interestingly,  $\text{SiC}_2$  silagraphene is a structural analogue of  $\text{B}_2\text{C}$  graphene:<sup>47</sup> substituting the alternating Si and C atoms entirely by C and B atoms transfers the  $\text{SiC}_2$  silagraphene into  $\text{B}_2\text{C}$  graphene. Wu et al.<sup>47</sup> have demonstrated that in  $\text{B}_2\text{C}$  the graphene B layer and C layer are separated by a tiny distance, which makes the sheet slightly corrugated. In contrast, the Si layer and C layer of the  $\text{SiC}_2$  silagraphene are in exactly the same plane.

It has been demonstrated that the 2D graphene<sup>58</sup> and Si graphene<sup>59</sup> are both semimetals with  $\pi$  and  $\pi^*$  states touching each other at the Fermi level. As a complex consisting of C and Si, what about the electronic structure of  $\text{SiC}_2$  silagraphene?

To answer this question, we computed the band structure and density of states (DOS) of  $\text{SiC}_2$  silagraphene (Figure 3a). Different from graphene and Si graphene,  $\text{SiC}_2$  silagraphene is metallic. The metallicity of  $\text{SiC}_2$  silagraphene is characterized by several energy levels crossing over from conduction band to valence band across the Fermi level in the band structure, as well as the peak at the Fermi level in the DOS. Analyzing the partial DOS reveals that the states at the Fermi level are mainly contributed by C-2p and Si-3p states, and C-2p contributes much more pronounced than Si-3p. Thus, the metallic property of  $\text{SiC}_2$  silagraphene mainly originates from the  $\pi$ -type  $\text{C}=\text{C}$  bonds.

Figure 3b and c present the highest occupied electronic state (HOES) and the lowest unoccupied electronic state (LUES) at the  $\Gamma$  point, respectively. The HOES clearly shows the strong bonding between Si and C atoms, while LUES is mainly contributed by the lone pair orbitals of the ptSi atoms, the same as in

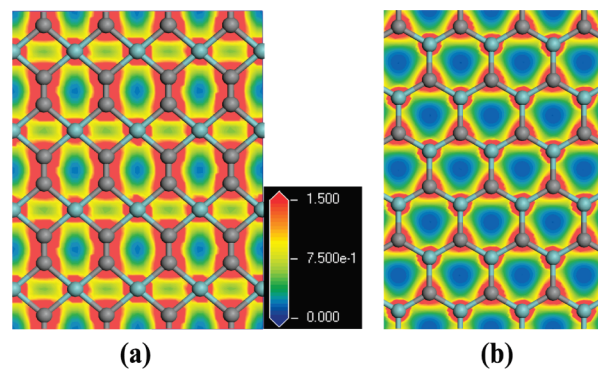


**Figure 4.** Total electronic charge density projected on the surface of (a)  $\text{SiC}_2$  silagraphene and (b) single-layered SiC sheet. The zero electron density is highlighted by blue.

the  $\text{SiC}_4$  building block, as removing the destabilizing ptSi lone pair electrons does help planarize the  $\text{SiC}_2$  silagraphene sheet.

To further understand the mechanism to stabilize ptSi in  $\text{SiC}_2$  silagraphene, we also studied a fenestrane-like structure  $\text{C}_{12}\text{H}_8\text{Si}$  with ptSi at the center<sup>26</sup> at the B3LYP/6-311+G\* level of theory (see the Supporting Information). In the planar  $D_{2h}$   $\text{C}_{12}\text{H}_8\text{Si}$ , the ptSi atom is positively charged (NPA charge 1.92) with the natural electron configuration of  $3s^{0.84}3p_x^{0.16}3p_y^{0.53}3p_z^{0.52}$ , and its LUMO corresponds to the destabilizing lone pair electrons of ptSi atom, similar to the case of  $\text{SiC}_4$  and the  $\text{SiC}_2$  silagraphene. Thus, one dominating factor to stabilize the ptSi arrangement in  $\text{SiC}_2$  silagraphene is the removal of lone pair electrons of ptSi atoms. However, the planar  $D_{2h}$   $\text{C}_{12}\text{H}_8\text{Si}$  is not a local minimum (with one imaginary frequency) and is 0.72 eV higher in energy than the true local minimum with  $D_2$  symmetry. This indicates the abundant  $\text{C}=\text{C}$  bonds that prefer planar skeletons also help stabilize the planar  $\text{SiC}_2$  network.

The metallic character of  $\text{SiC}_2$  silagraphene also reminds us of the previously predicted semiconducting characteristics of graphitic single-layered SiC. Although also consisting of Si and C, the SiC sheet was computed to have a  $\sim$ 2.5 eV band gap.<sup>60</sup> What makes the difference in the electronic properties between  $\text{SiC}_2$  and SiC sheet? First, the  $\pi$ -type  $\text{C}=\text{C}$  bonds, which govern the metallicity of  $\text{SiC}_2$  silagraphene, are absent in the SiC sheet. Second, the valence electrons are distributed differently in the  $\text{SiC}_2$  and SiC sheets, as indicated by their charge densities (Figure 4). The valence electrons in  $\text{SiC}_2$  silagraphene are uniformly distributed, and the zero-electron holes are negligible. In contrast, the valence electrons in SiC sheet are mainly localized between Si and C atoms, and there are many zero-electron holes, thereby depressing the probability of electron conduction as compared with those in  $\text{SiC}_2$  silagraphene.

**3.3. Stability of  $\text{SiC}_2$  Silagraphene.** Is this currently hypothetical  $\text{SiC}_2$  silagraphene stable, or more precisely, viable?<sup>61</sup> The answer is yes. First,  $\text{SiC}_2$  silagraphene sheet is a local minimum. No imaginary frequencies are found in the frequency computations by using DMol<sup>3</sup> code with DND basis set and by using the Vienna ab initio simulation package (VASP)<sup>62</sup> with a plane-wave pseudopotential method.<sup>63</sup> Second,  $\text{SiC}_2$  silagraphene has a relatively large binding energy (6.04 eV/atom), which shows the strong covalent bonds in the sheet. As a reference, the binding energies of SiC solid (6H), graphene, Si solid, and the low-buckled Si sheet<sup>64</sup> are 6.51, 8.66, 4.57, and 3.93 eV/atom, respectively. Interestingly, the binding energy of  $\text{SiC}_2$  silagraphene coincides with that of the single-layer SiC sheet.

This is a little surprising because the Si–C bond in the ptSi-containing  $\text{SiC}_2$  sheet is weaker than that in the single-layer SiC sheet, which is suggested by the computed Mülliken bond orders (0.72 and 0.93, respectively). However, the abundance of strong CC bonds (Mülliken bond order of 1.39) in  $\text{SiC}_2$  sheet substantially compensates the relatively weak SiC bonds, thus leading to the comparable binding energies of  $\text{SiC}_2$  and SiC sheets. Third, the kinetic stability of  $\text{SiC}_2$  silagraphene is considerably high, as indicated by our MD simulations at the DFT level of theory. We performed three MD simulations, at 300, 800, and 1000 K (each for 10 ps). The snapshot images of the equilibrium structure at the end of each MD simulation are shown in Figure S1 (see the Supporting Information). At 300 K, the geometry of  $\text{SiC}_2$  silagraphene is well kept; at 800 K, the structure can still be intact for 10 ps; only at 1000 K is the  $\text{SiC}_2$  planar structure seriously folded and melted: many Si–C bonds are broken and most ptSi atoms change into tricoordinated. These MD simulations suggest that the  $\text{SiC}_2$  sheet likely melts at a temperature between 800 and 1000 K. Finally, to further test the thermodynamic stability of  $\text{SiC}_2$  silagraphene, we performed optimizations starting from the distorted structures after MD simulations. After full atomic relaxation, the distorted structures from 300 and 800 K can easily recover the planar  $\text{SiC}_2$  structure, while that annealed at 1000 K cannot. Accordingly, once formed,  $\text{SiC}_2$  silagraphene can maintain its structural integrity at least up to 800 K.

The experimental realization of such a rule-breaking material is challenging. A promising approach is to produce the  $\text{SiC}_2$  silagraphene on the surface of suitable compound crystals by chemical vapor deposition method, in which these surfaces serve as both catalysts and templates. This approach is similar to what was used to synthesize large-area graphene films.<sup>65</sup>

Selecting a good template whose lattice structure matches that of  $\text{SiC}_2$  silagraphene is the key to achieve the  $\text{SiC}_2$  silagraphene sheet. Our preliminary screening indentified that the [100] and [010] surfaces of tetragonal PdO (P42/MMC) may help solve this problem (see the Supporting Information), and we propose that the  $\text{SiC}_2$  silagraphene can be achieved by indirect assembly on the PdO [1 0 0] and [0 1 0] surfaces.

**3.4. Structural and Electronic Properties of  $\text{SiC}_2$  Nanotubes.** Tubular structures of  $\text{SiC}_2$  can be constructed by rolling up the  $\text{SiC}_2$  silagraphene sheet along specific directions in the 2D lattice, in the same way to get a single-walled carbon nanotube from a graphene layer. Like carbon nanotubes,<sup>66</sup>  $\text{SiC}_2$  nanotubes can be indexed by a pair of integers  $(n,m)$ , corresponding to a lattice vector  $L = na + mb$  on the  $\text{SiC}_2$  plane, where  $a$  and  $b$  are the unit cell vectors of the  $\text{SiC}_2$  sheet (Figure 2a).

In Figure 5, we show two representative  $\text{SiC}_2$  nanotubes, (10,0) and (0,10). The unit-cell lengths in the axial direction are 3.906 and 2.816 Å, respectively, for these two nanotubes. The lengths of the Si–C bond (1.914 and 1.910 Å for (10,0) and (0,10) tube, respectively) and C=C bond (1.328 and 1.330 Å for (10,0) and (0,10) tube, respectively) are quite close to those of  $\text{SiC}_2$  silagraphene. The charge transfer from Si (1.14 and 1.19 e for (10,0) and (0,10) tube, respectively) to C is less than that in the  $\text{SiC}_2$  silagraphene. The same as their 2D analogues, both (10,0) and (0,10)  $\text{SiC}_2$  nanotubes are metallic, as indicated by the computed band structures (Figure 5).

We also computed a variety of other  $(n,0)$  and  $(0,n)$   $\text{SiC}_2$  nanotubes with a diameter ranging between 5 and 20 Å, which correspond to indices from (6,0)–(0,6) to (15,0)–(0,15) (see Table S1 in the Supporting Information). In all the  $(n,0)$  and  $(0,n)$   $\text{SiC}_2$  tubes that we examined, the optimized bond lengths

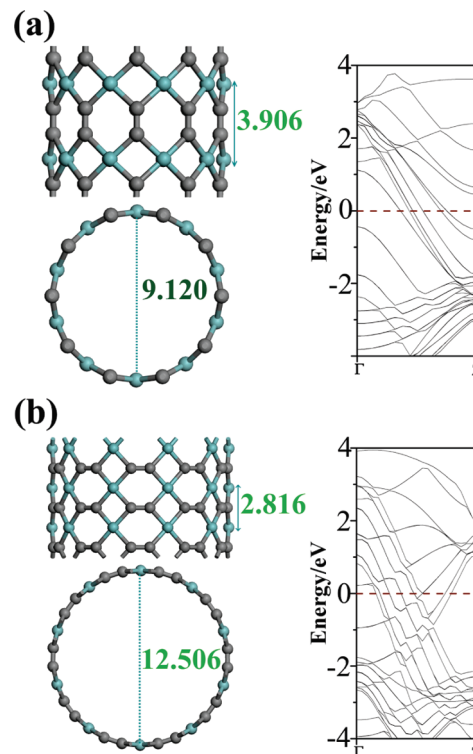


**Figure 5.** Side (left upper) and top (left lower) views of optimized structures and corresponding electronic band structures for (a) (10,0) and (b) (0,10)  $\text{SiC}_2$  nanotubes.

are very close to those of the planar sheet, even for those highly curved thin tubes. The charge transfer from Si to C increases with increasing the tube diameter and approaches that of the  $\text{SiC}_2$  silagraphene. Especially, regardless of the roll-up vector, all  $\text{SiC}_2$  tubes are metallic. This is in stark contrast to the conventional  $(n,m)$  carbon nanotubes and SiC nanotubes: carbon nanotubes are metallic only if  $(n-m)/3$  is an integer, otherwise they are semiconducting with a band gap,<sup>67</sup> and the SiC nanotubes are generally semiconductors.<sup>68</sup> The chirality-independent metallicity of  $\text{SiC}_2$  nanotubes also strikingly differs from that of the isostructural  $\text{B}_2\text{C}$  nanotubes: Wu et al.<sup>47</sup> reported that the  $\text{B}_2\text{C}$  nanotubes may be either a metal or a semiconductor, depending on the roll-up vector.

**3.5. Stability of  $\text{SiC}_2$  Nanotubes.** Are the  $\text{SiC}_2$  nanotubes stable? To evaluate the stability of these nanotubes, we computed their strain energies and binding energies and compared these values with those of the experimentally available carbon and boron nitride (BN) nanotubes, as well as the single-walled SiC nanotubes.

Figure 6a presents the strain energies of  $(n,0)$  and  $(0,n)$   $\text{SiC}_2$  nanotubes as a function of the tube diameters. For both  $(n,0)$  and  $(0,n)$   $\text{SiC}_2$  nanotubes, the strain energy decreases monotonically with increasing tube diameters and approaches zero gradually. With comparable diameters, the  $(n,0)$  nanotubes are of lower strain energies, and are thus easier to form from the silagraphene sheet.

We also computed the strain energies of a series of carbon, BN, and SiC nanotubes and compared them with those of  $\text{SiC}_2$  nanotubes (Figure 6a). Noticeably, both  $(n,0)$  and  $(0,n)$   $\text{SiC}_2$  nanotubes have smaller strain energies than the single-walled carbon and SiC nanotubes with similar diameters. When compared with

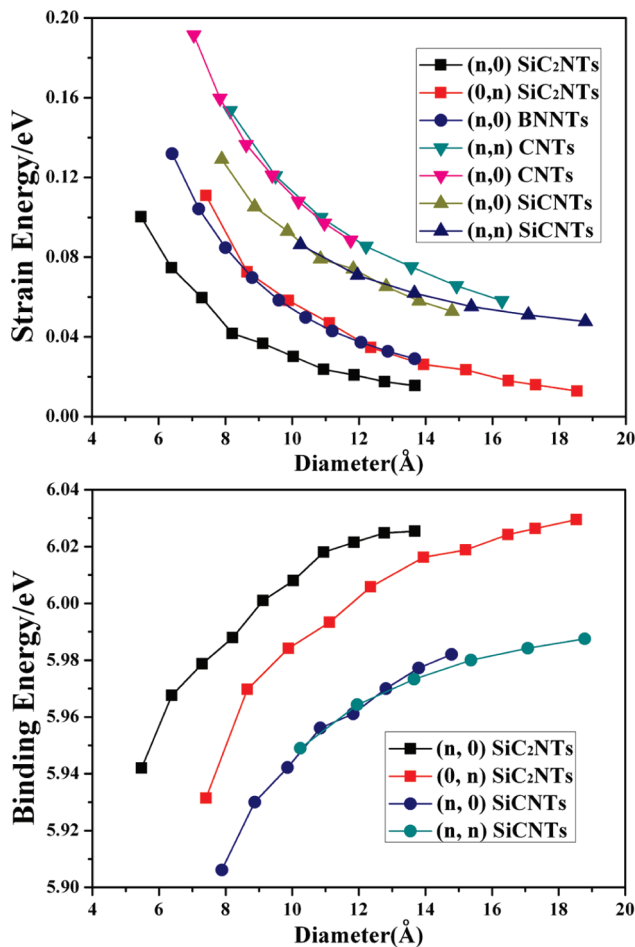


**Figure 6.** Variation of (a) the strain energy and (b) the binding energy of  $(n,0)$  ( $6 \leq n \leq 15$ ) and  $(0,n)$  ( $6 \leq n \leq 15$ )  $\text{SiC}_2$  nanotubes as a function of tube diameter. For a comparison, in (a), the strain energies of a series of  $(n,0)$  ( $8 \leq n \leq 17$ ) BN nanotube,  $(n,0)$  ( $9 \leq n \leq 15$ ) and  $(n,n)$  ( $6 \leq n \leq 12$ ) carbon nanotubes, and  $(n,0)$  ( $8 \leq n \leq 15$ ) and  $(n,n)$  ( $6 \leq n \leq 11$ )  $\text{SiC}$  nanotubes are computed; in (b), the binding energies of  $(n,0)$  ( $8 \leq n \leq 15$ ) and  $(n,n)$  ( $6 \leq n \leq 11$ )  $\text{SiC}$  nanotubes are also computed.

the BN nanotubes with comparable diameters, the  $(0,n)$   $\text{SiC}_2$  nanotubes have nearly equivalent strain energies, while the  $(n,0)$   $\text{SiC}_2$  nanotubes are much less strained. Thus, the  $\text{SiC}_2$  nanotubes are of the least strain among these nanotubes and can be rolled up with the least energy cost from the 2D nanosheet.

Furthermore, the relative stability of  $\text{SiC}_2$  nanotube can also be hinted by their binding energies (Figure 6b). Our results demonstrate that the binding energies of  $\text{SiC}_2$  nanotubes are larger than those of single-walled  $\text{SiC}$  nanotubes with comparable diameters. The binding energy differences between  $\text{SiC}_2$  and  $\text{SiC}$  nanotubes decrease with increasing tube diameters and will diminish when the diameters are infinitely large (in the case of the planar sheet form, where the  $\text{SiC}_2$  silagraphene has the same binding energy (6.04 eV/atom) as the single-layer  $\text{SiC}$  sheet). Note that silicon carbide nanotubes have been experimentally realized, for example, by chemical vapor deposition,<sup>69</sup> or reacting silicon source with multiwalled carbon nanotubes (also as templates),<sup>70</sup> although the detailed structure of the synthesized nanotubes was not fully resolved.

These energetic analyses show that the  $\text{SiC}_2$  nanotubes are less strained when compared with the experimentally available carbon,

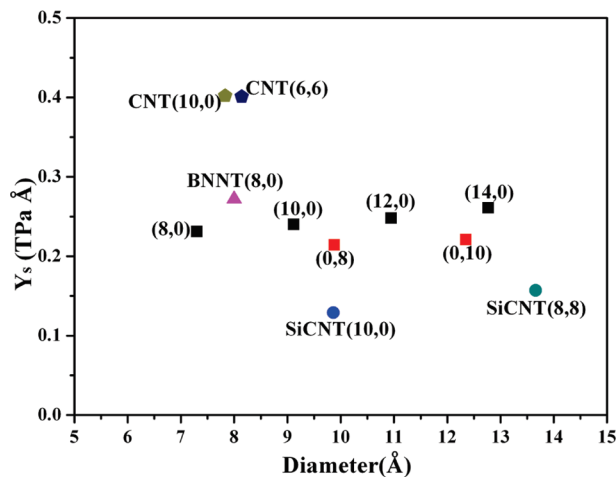


**Figure 7.** Computed Young's modulus ( $Y_s$ ) of  $\text{SiC}_2$ ,  $\text{SiC}$ , BN, and carbon nanotubes. The  $(n,0)$  and  $(0,n)$   $\text{SiC}_2$  nanotubes are denoted with black and red “■”, respectively.

BN, and  $\text{SiC}$  nanotubes and are also of significantly large binding energies. Thus, although at present  $\text{SiC}_2$  nanotubes have not been observed experimentally, we believe that they hold promising potential to be synthesized under some appropriate experimental conditions.

**3.6. Elastic Properties of  $\text{SiC}_2$  Nanotubes.** To assess the mechanical properties, which are important for many applications, we evaluated the elastic properties of  $\text{SiC}_2$  nanotubes by computing their Young's modulus ( $Y_s$ ) as proposed by Hernández et al.<sup>54</sup> Here, six  $\text{SiC}_2$  nanotubes were computed, including  $(8,0)$ ,  $(10,0)$ ,  $(12,0)$ ,  $(14,0)$ ,  $(0,8)$ , and  $(0,12)$  nanotubes. In addition, the zigzag  $(10,0)$  and armchair  $(6,6)$  carbon nanotubes,  $(10,0)$  BN nanotube, and  $(10,0)$  and  $(8,8)$   $\text{SiC}$  nanotubes were considered for comparison. Our computed  $Y_s$  values of carbon and BN nanotubes are in good coincidence with previous studies.<sup>54</sup>

Examining the computed  $Y_s$  values (Figure 7) led to the following conclusions: (1) the elastic moduli  $Y_s$ 's of  $\text{SiC}_2$  nanotubes are sensitive to the size and the helicity, which is in sharp contrast to carbon nanotubes; (2) the  $Y_s$ 's of both  $(n,0)$  and  $(0,n)$   $\text{SiC}_2$  tubes increase with increasing tube diameters, and the  $(n,0)$  nanotubes have larger  $Y_s$  than the  $(0,n)$  nanotubes with similar diameters; and (3) when the tubes are of comparable wall thickness, the elastic moduli of  $\text{SiC}_2$  nanotubes is at the same order of other nanotubes considered here, although smaller than carbon nanotubes; they are comparable to those of BN nanotubes and larger than those of  $\text{SiC}$  nanotubes. All these results indicate that  $\text{SiC}_2$  nanotubes have rather good elastic properties.

**3.7. Electronic Properties of  $\text{SiC}_2$  Nanoribbons.** Finally, inspired by the intensive studies of graphene nanoribbons (GNRs) and their attractive electronic properties for the nanoelectronics,<sup>71,72</sup> we investigated the electronic properties of  $\text{SiC}_2$  nanoribbons.

Two types of  $\text{SiC}_2$  nanoribbons can be obtained by cutting  $\text{SiC}_2$  silagraphene along the different directions ( $a$  or  $b$  axis), and they can have different widths and terminating atoms (C and Si). Figure 8 presents some representative examples, while more nanoribbons are given in the Supporting Information. After atomic relaxation, all atoms (Si, C, and H) are still in the same plane, and the lattice parameters  $a$  and  $b$  only change slightly as compared with those of  $\text{SiC}_2$  silagraphene (less than 0.01 Å). The same as the 2D sheet and 1D nanotubes, all these  $\text{SiC}_2$  nanoribbons

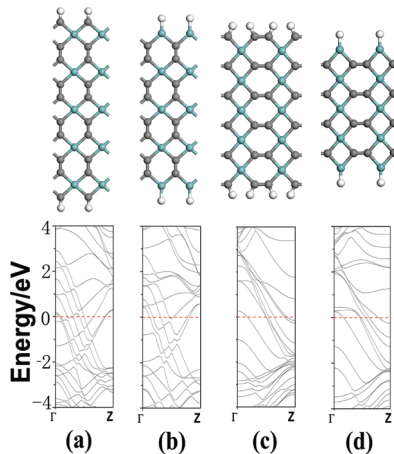


**Figure 8.** Optimized geometry structures and corresponding band structures of (a) type-I-C-5, (b) type-I-Si-3, (c) type-II-C-5, and (d) type-II-Si-3  $\text{SiC}_2$  nanoribbons. Type-I and type-II indicate that these  $\text{SiC}_2$  nanoribbons are cut along the  $a$  and  $b$  axes, respectively. C and Si denote that edge sites of  $\text{SiC}_2$  nanoribbons are occupied with C and Si atoms, respectively. Each edge atom is passivated with a hydrogen atom (white ball). Width parameters of 5 and 3 represent the number of ptSi atoms.

are metallic with several energy levels crossing over from conduction band to valence band across the Fermi level, independent of the ribbon width and edge structure. It is in striking contrast to GNRs and SiC nanoribbons: GNRs all have a nonzero energy gap, while SiC nanoribbons<sup>60a</sup> can be either nonmagnetic semiconductors (for armchair ribbons) or magnetic metals (for zigzag ribbons), and the very narrow zigzag nanoribbons can be even half-metallic.

#### 4. CONCLUSION

In summary, our systematic DFT computations expanded planar tetracoordinate silicon (ptSi) into periodic systems: a  $C_{2v}$   $\text{SiC}_4$  building block was identified, followed by the construction of the infinite  $\text{SiC}_2$  silagraphene, essentially a 2D network of  $\text{SiC}_4$ ; then, the 1D  $\text{SiC}_2$  nanotubes and nanoribbons were built up by rolling up or cutting the 2D  $\text{SiC}_2$  silagraphene sheet. We attribute the fundamental mechanism of forming the ptSi networks in  $\text{SiC}_2$  silagraphene to the following two factors: (1) the removal of the destabilizing ptSi lone pair electrons that significantly stabilizes the ptSi arrangement; and (2) the abundance of  $\text{C}=\text{C}$  bonds that yield planarity-preferred ethylene-like skeletons and give rise to a planar  $\text{SiC}_2$  network. The  $\text{SiC}_2$  silagraphene is a stable phase, being a local minimum in the potential energy surface, and having the same binding energy as SiC silagraphene and rather high kinetic and thermodynamic stabilities. The  $\text{SiC}_2$  nanotubes are also rather stable, as indicated by their smaller strain energies and rather large binding energies, and have excellent elastic properties. All these ptSi-containing nanomaterials, ranging from silagraphene, nanotubes, to nanoribbons, are metallic, which is contrast to their carbon and SiC analogues. We also proposed a promising approach to synthesize the  $\text{SiC}_2$  silagraphene by indirect assembly on the PdO [100] and [010] surfaces.

These studies not only put forward the novel chemical bonding, planar tetracoordinate silicon, into nanomaterials, but also lead to highly stable new silicon carbide phases with unique electronic properties for future experimental realization. We hope that our studies will inspire experimental and theoretical studies

on  $\text{SiC}_2$  silagraphene and its 1D derivatives, and also more efforts in investigating nanomaterials with novel chemical bonding, and we anticipate that these rule-breaking systems will soon join the glorious nanomaterials family.

#### ■ ASSOCIATED CONTENT

**S Supporting Information.** Low-energy isomers of  $\text{SiC}_4$  cluster and their relative energies, snapshots of MD simulation, geometrics and canonical molecular orbitals of fenestrane-like structure  $\text{C}_{12}\text{H}_8\text{Si}$ , structural properties of a series of  $\text{SiC}_2$  nanotubes, geometric and electronic structures of  $\text{SiC}_2$  nanoribbons with different widths, the SiC bond lengths in the bulk materials, complete citation of ref 50, and the proposed approach to synthesize  $\text{SiC}_2$  silagraphene. This material is available free of charge via the Internet at <http://pubs.acs.org>.

#### ■ AUTHOR INFORMATION

##### Corresponding Author

zhouzhen@nankai.edu.cn; zhongfangchen@gmail.com

#### ■ ACKNOWLEDGMENT

Support in China by NSFC (21073096) and MOE NCET (08-0293) and Innovation Team (IRT0927), and in the U.S. by NSF Grant CHE-0716718 and the FIP grant of University of Puerto Rico, is gratefully acknowledged. This research was also supported in part by the National Science Foundation through TeraGrid resources. We thank the anonymous referees for valuable suggestion.

#### ■ REFERENCES

- (1) Kroto, H. W.; Heath, J. R.; O'Brien, S. C.; Curl, R. F.; Smalley, R. E. *Nature* **1985**, *318*, 162.
- (2) Iijima, S. *Nature* **1991**, *354*, 56.
- (3) Iijima, S.; Ichihashi, T. *Nature* **1993**, *363*, 603.
- (4) Novoselov, K. S.; Geim, A. K.; Morozov, S. V.; Jiang, D.; Zhang, Y.; Dubonos, S. V.; Grigoreva, I. V.; Firsov, A. A. *Science* **2004**, *306*, 666.
- (5) Katsnelson, M. I.; Novoselov, K. S.; Geim, A. K. *Nat. Phys.* **2006**, *2*, 620.
- (6) Katsnelson, M. I.; Novoselov, K. S. *Solid State Commun.* **2007**, *143*, 3.
- (7) Novoselov, K. S.; Jiang, Z.; Zhang, Y.; Morozov, S. V.; Stormer, H. L.; Zeitler, U.; Maan, J. C.; Boebinger, G. S.; Kim, P.; Geim, A. K. *Science* **2007**, *315*, 1379.
- (8) Zhang, Y.; Tan, Y.-W.; Stormer, H. L.; Kim, P. *Nature* **2005**, *438*, 201.
- (9) Morozov, S. V.; Novoselov, K. S.; Katsnelson, M. I.; Schedin, F.; Elias, D.; Jaszczak, J. A.; Geim, A. K. *Phys. Rev. Lett.* **2008**, *100*, 016602.
- (10) Lee, C. G.; Wei, X. D.; Kysar, J. W.; Hone, J. *Science* **2008**, *321*, 385.
- (11) Elias, D. C.; Nair, R. R.; Mohiuddin, T. M. G.; Morozov, S. V.; Blake, P.; Halsall, M. P.; Ferrari, A. C.; Boukhvalov, D. W.; Katsnelson, M. I.; Geim, A. K.; Novoselov, K. S. *Science* **2009**, *323*, 610.
- (12) (a) Hoffmann, R.; Alder, R. W.; Wilcox, C. F., Jr. *J. Am. Chem. Soc.* **1970**, *92*, 4992. (b) Hoffmann, R. *Pure Appl. Chem.* **1971**, *28*, 181.
- (13) (a) van't Hoff, J. H.; Neerl, A. *Sci. Exactes Nat.* **1874**, 445. (b) Le Bel, J. A. *Bull. Soc. Chim. Fr.* **1874**, *22*, 337.
- (14) Collins, J. B.; Dill, J. D.; Jemmis, E. D.; Apeloig, Y.; Schleyer, P. v. R.; Seeger, R.; Pople, J. A. *J. Am. Chem. Soc.* **1976**, *98*, 5419.
- (15) Cotton, F. A.; Millar, M. *J. Am. Chem. Soc.* **1977**, *99*, 7886.
- (16) Keese, R.; Pfenniger, A.; Roesle, A. *Helv. Chim. Acta* **1979**, *62*, 326.
- (17) For recent reviews, see: (a) Sorger, K.; Schleyer, P. v. R. *J. Mol. Struct. (THEOCHEM)* **1995**, *338*, 317. (b) Radom, L.; Rasmussen, D. R.

- Pure Appl. Chem.* **1998**, *70*, 1977. (c) Siebert, W.; Gunale, A. *Chem. Soc. Rev.* **1999**, *28*, 367. (d) Keesee, R. *Chem. Rev.* **2006**, *106*, 4787. (e) Merino, G.; Mendez-Rojas, M. A.; Vela, A.; Heine, T. *J. Comput. Chem.* **2007**, *28*, 362. (f) Boldyrev, A. I.; Wang, L. S. *J. Phys. Chem. A* **2001**, *105*, 10759.
- (18) (a) Wang, Z. X.; Schleyer, P. v. R. *Science* **2001**, *292*, 2465. (b) Exner, K.; Schleyer, P. v. R. *Science* **2000**, *290*, 1937. (c) Ito, K.; Chen, Z. F.; Corminboeuf, C.; Wannere, C. S.; Zhang, X. H.; Li, Q. S.; Schleyer, P. v. R. *J. Am. Chem. Soc.* **2007**, *129*, 1510. (d) Wang, Z.-X.; Schleyer, P. v. R. *Angew. Chem., Int. Ed.* **2002**, *41*, 4082. (e) Pei, Y.; An, W.; Ito, K.; Schleyer, P. v. R.; Zeng, X. C. *J. Am. Chem. Soc.* **2008**, *130*, 10394.
- (19) (a) Wang, L. M.; Huang, W.; Averkiev, B. B.; Boldyrev, A. I.; Wang, L. S. *Angew. Chem., Int. Ed.* **2007**, *46*, 4550. (b) Averkiev, B. B.; Zubarev, D. Y.; Wang, L. M.; Huang, W.; Wang, L. S.; Boldyrev, A. I. *J. Am. Chem. Soc.* **2008**, *130*, 9248. (c) Averkiev, B. B.; Wang, L. M.; Huang, W.; Wang, L. S.; Boldyrev, A. I. *Phys. Chem. Chem. Phys.* **2009**, *11*, 9840.
- (20) Wang, Y.; Robinson, G. H. *Chem. Commun.* **2009**, 5201.
- (21) Kost, D.; Kalikhman, I. *Acc. Chem. Res.* **2009**, *42*, 303.
- (22) Jemmis, E. D.; Jayasree, E. G.; Parameswaran, P. *Chem. Soc. Rev.* **2006**, *35*, 157.
- (23) Wurthwein, E.-U.; Schleyer, P. v. R. *Angew. Chem., Int. Ed. Engl.* **1979**, *18*, 553.
- (24) Meyer, H.; Nagorsen, G. *Angew. Chem., Int. Ed. Engl.* **1979**, *18*, 551.
- (25) (a) Dunitz, J. D. *Angew. Chem., Int. Ed. Engl.* **1980**, *19*, 1034. (b) Nagorsen, G.; Meyer, H. *Angew. Chem., Int. Ed. Engl.* **1980**, *19*, 1034. (c) Schomburg, D. *Angew. Chem., Int. Ed. Engl.* **1983**, *22*, 65. (d) Hönlé, W.; Dettlaff-Weglikowska, U.; Walz, L.; von Schnerring, H. G. *Angew. Chem., Int. Ed. Engl.* **1989**, *28*, 623.
- (26) Boldyrev, A. I.; Schleyer, P. v. R.; Keesee, R. *Mendeleev Commun.* **1992**, 93.
- (27) Ding, B.; Keesee, R.; Stoeckli-Evans, H. *Angew. Chem., Int. Ed.* **1999**, *38*, 375.
- (28) Schleyer, P. v. R.; Reed, A. E. *J. Am. Chem. Soc.* **1988**, *110*, 4453.
- (29) (a) Belanzoni, P.; Giorgi, G.; Cerofolini, G. F.; Sgamellotti, A. *J. Phys. Chem. A* **2006**, *110*, 4582. (b) Belanzoni, P.; Giorgi, G.; Cerofolini, G. F.; Sgamellotti, A. *Theor. Chem. Acc.* **2006**, *115*, 448.
- (30) Tiznado, W.; Perez-Peralta, N.; Islas, R.; Toro-Labbe, A.; Ugalde, J. M.; Merino, G. *J. Am. Chem. Soc.* **2009**, *131*, 9426.
- (31) Gribanova, T. N.; Minyaev, R. M.; Minkin, V. I. *Russ. J. Gen. Chem.* **2005**, *75*, 1651.
- (32) Islas, R.; Heine, T.; Ito, K.; Schleyer, P. v. R.; Merino, G. *J. Am. Chem. Soc.* **2007**, *129*, 14767.
- (33) Szieberth, D.; Takahashi, M.; Kawazoe, Y. *J. Phys. Chem. A* **2009**, *113*, 707.
- (34) Guo, J.-C.; Li, S.-D. *J. Mol. Struct. (THEOCHEM)* **2007**, *816*, 59.
- (35) (a) Li, S. D.; Ren, G. M.; Miao, C. Q. *Inorg. Chem.* **2004**, *43*, 6331. (b) Li, S. D.; Miao, C. Q. *J. Phys. Chem. A* **2005**, *109*, 7594.
- (36) (a) Li, S.-D.; Miao, C.-Q.; Guo, J.-C.; Ren, G.-M. *J. Am. Chem. Soc.* **2004**, *126*, 16227. (b) Li, S.-D.; Guo, J.-C.; Miao, C.-Q.; Ren, G.-M. *J. Phys. Chem. A* **2005**, *109*, 4133.
- (37) Boldyrev, A. I.; Li, X.; Wang, L.-S. *Angew. Chem., Int. Ed.* **2000**, *39*, 3307.
- (38) Krogh-Jespersen, M.-B.; Chandrasekhar, J.; Würthwein, E.-U.; Collins, J. B.; Schleyer, P. v. R. *J. Am. Chem. Soc.* **1980**, *102*, 2263.
- (39) Pancharatna, P. D.; Méndez-Rojas, M. A.; Merino, G.; Vela, A.; Hoffmann, R. *J. Am. Chem. Soc.* **2004**, *126*, 15309.
- (40) (a) Merino, G.; Méndez-Rojas, M. A.; Beltran, H. I.; Corminboeuf, C.; Heine, T.; Vela, A. *J. Am. Chem. Soc.* **2004**, *126*, 16160. (b) Merino, G.; Méndez-Rojas, M. A.; Vela, A. *J. Am. Chem. Soc.* **2003**, *125*, 6026.
- (41) Yang, L. M.; Ding, Y. H.; Sun, C. C. *J. Am. Chem. Soc.* **2007**, *129*, 658.
- (42) Zhang, C. J.; Sun, W. X.; Cao, Z. X. *J. Am. Chem. Soc.* **2008**, *130*, 5638.
- (43) Wu, Y. B.; Yuan, C. X.; Gao, F.; Lu, H. G.; Guo, J. C.; Li, S. D.; Wang, Y. K.; Yang, P. *Organometallics* **2007**, *26*, 4395.
- (44) Wu, Y. B.; Jiang, J. L.; Zhang, E. W.; Wang, Z. X. *Chem.-Eur. J.* **2010**, *16*, 1271.
- (45) Wu, M. H.; Pei, Y.; Zeng, X. C. *J. Am. Chem. Soc.* **2010**, *132*, 5554.
- (46) Pei, Y.; Zeng, X. C. *J. Am. Chem. Soc.* **2008**, *130*, 2580.
- (47) Wu, X. J.; Pei, Y.; Zeng, X. C. *Nano Lett.* **2009**, *9*, 1577.
- (48) (a) Becke, A. D. *J. Chem. Phys.* **1993**, *98*, 5648. (b) Lee, C.; Yang, W.; Parr, R. G. *Phys. Rev. B: Condens. Mater. Phys.* **1988**, *37*, 785. (c) Clark, T.; Chandrasekhar, J.; Spitznagel, G. W.; Schleyer, P. v. R. *J. Comput. Chem.* **1983**, *4*, 294. (d) Frisch, M. J.; Pople, J. A.; Binkley, J. S. *J. Chem. Phys.* **1984**, *80*, 3265.
- (49) (a) Head-Gordon, M.; Pople, J. A. *Chem. Phys. Lett.* **1988**, *153*, 503. (b) Frisch, M. J.; Head-Gordon, M.; Pople, J. A. *Chem. Phys. Lett.* **1990**, *166*, 275. (c) Frisch, M. J.; Head-Gordon, M.; Pople, J. A. *Chem. Phys. Lett.* **1990**, *166*, 281.
- (50) Frisch, M. J.; et al. *Gaussian 03*, revision E.02; Gaussian, Inc.: Wallingford, CT, 2004. See the Supporting Information for the full reference.
- (51) (a) Delley, B. *J. Chem. Phys.* **1990**, *92*, 508. (b) Delley, B. *J. Chem. Phys.* **2000**, *113*, 7756.
- (52) Perdew, J. P.; Wang, Y. *Phys. Rev. B* **1992**, *45*, 13244.
- (53) Martyna, G. J.; Klein, M. L.; Tuckerman, M. E. *J. Chem. Phys.* **1992**, *97*, 2635.
- (54) Hernández, E.; Goze, C.; Bernier, P.; Rubio, A. *Phys. Rev. Lett.* **1998**, *80*, 4502.
- (55) (a) Head-Gordon, M.; Pople, J. A. *Chem. Phys. Lett.* **1988**, *153*, 503. (b) Frisch, M. J.; Head-Gordon, M.; Pople, J. A. *Chem. Phys. Lett.* **1990**, *166*, 275. (c) Frisch, M. J.; Head-Gordon, M.; Pople, J. A. *Chem. Phys. Lett.* **1990**, *166*, 281.
- (56) Wang, Z. X.; Schleyer, P. v. R. *J. Am. Chem. Soc.* **2002**, *124*, 11979.
- (57) (a) Bazant, V.; Chvalovsky, V.; Rathousky, J. *Organosilicon Compounds*; Academic Press: New York, 1965; p 179. (b) Gordon, A. J.; Ford, R. A. *The Chemist's Companion*; Wiley: New York, 1972; p 107. (c) Thibault, N. W. *Am. Mineral.* **1944**, *29*, 327. (d) Tomaszewski, P. E. *Phase Transitions* **1992**, *38*, 127. (e) Schulz, H.; Thiemann, K. H. *Solid State Commun.* **1979**, *32*, 783.
- (58) Wallace, P. R. *Phys. Rev.* **1947**, *71*, 622.
- (59) Cahangirov, S.; Topsakal, M.; Aktürk, Şahin, H.; Ciraci, S. *Phys. Rev. Lett.* **2009**, *102*, 236804.
- (60) (a) Sun, L.; Li, Y. F.; Li, Z. F.; Li, Q. X.; Zhou, Z.; Chen, Z. F.; Yang, J. L.; Hou, J. G. *J. Chem. Phys.* **2008**, *129*, 174114. (b) Bekaroglu, E.; Topsakal, M.; Cahangirov, S.; Ciraci, S. *Phys. Rev. B* **2010**, *81*, 075433.
- (61) Hoffmann, R.; Schleyer, P. v. R.; Schaefer, H. F., III. *Angew. Chem., Int. Ed.* **2008**, *47*, 7164.
- (62) Kresse, G.; Furthmuller, J. *Phys. Rev. B* **1996**, *54*, 11169.
- (63) Our theoretical computations were performed with the generalized gradient approximation (GGA) PW91 functional, and interaction between ions and electrons using the frozen-core projector augmented wave approach. The plane-wave basis set cutoff is 400 eV.
- (64) Cahangirov, S.; Topsakal, M.; Aktürk, E.; Şahin, H.; Ciraci, S. *Phys. Rev. Lett.* **2009**, *102*, 236804.
- (65) (a) Li, X. S.; Cai, W. W.; An, J. H.; Kim, S.; Nah, J.; Yang, D. X.; Pineri, R. D.; Velamakanni, A.; Jung, I.; Tutuc, E.; Banerjee, S. K.; Colombo, L.; Ruoff, R. S. *Science* **2009**, *324*, 1312. (b) Hofrichter, J.; Szafranek, B. N.; Otto, M.; Echtermeyer, T. J.; Baus, M.; Majerus, A.; Geringer, V.; d Ramsteiner, M.; Kurz, H. *Nano Lett.* **2010**, *10*, 36.
- (66) White, C. T.; Robertson, D. H.; Mintmire, J. W. *Phys. Rev. B* **1993**, *47*, 5485.
- (67) Yamabe, T. *Synth. Met.* **1995**, *70*, 1511.
- (68) (a) Zhao, M.; Xia, Y.; Li, F.; Zhang, R. Q.; Lee, S. T. *Phys. Rev. B* **2005**, *71*, 085312. (b) Wu, J. J.; Guo, G. Y. *Phys. Rev. B* **2007**, *76*, 035343. (c) Yu, M.; Jayanthi, C. S.; Wu, S. Y. *Phys. Rev. B* **2010**, *82*, 075407.
- (69) Xie, Z.; Tao, D.; Wang, J. *J. Nanosci. Nanotechnol.* **2007**, *7*, 647.
- (70) (a) Sun, X. H.; Li, C. P.; Wong, W. K.; Wong, N. B.; Lee, C. S.; Lee, S. T.; Teo, B. K. *J. Am. Chem. Soc.* **2002**, *124*, 14464. (b) Taguchi,

T.; Igawa, N.; Yamamoto, H.; Jitsukawa, S. *J. Am. Chem. Soc.* **2005**, 88, 459. (c) Keller, N.; Pham-Huu, C.; Ehret, G.; Keller, V.; Ledoux, M. J. *Carbon* **2003**, 41, 2131.

(71) For recent reviews, see: (a) Geim, A. K.; Novoselov, K. S. *Nat. Mater.* **2007**, 6, 183. (b) Fukui, K.-I.; Kobayashi, Y.; Enoki, T. *Int. Rev. Phys. Chem.* **2007**, 26, 609.

(72) (a) Son, Y. W.; Cohen, M. L.; Louie, S. G. *Nature* **2006**, 444, 347. (b) Barone, V.; Hod, O.; Scuseria, G. E. *Nano Lett.* **2006**, 6, 2748.